Polaronic effect in the x-ray absorption spectra of $La_{1-x}Ca_xMnO_3$ manganites

S W Huang[1,2,3], Y T Liu[4], J M Lee[1,5], J M Chen[5], J F Lee[5], R W Schoenlein[3,6], Y-D Chuang[2] and J-Y Lin[4,7]

[1] MAX IV Laboratory, Lund University, PO Box 118, 221 00 Lund, Sweden
[2] Advanced Light Source, Lawrence Berkeley National Laboratory, Berkeley, CA 94720, United States of America
[3] Materials Sciences Division, Lawrence Berkeley National Laboratory, Berkeley, CA 94720, United States of America
[4] Institute of Physics, National Chiao Tung University, Hsinchu 300, Taiwan
[5] National Synchrotron Radiation Research Center, Hsinchu 30076, Taiwan
[6] Linac Coherent Light Source, SLAC National Accelerator Laboratory, Menlo Park, CA 94035, United States of America
[7] Center for Emergent Functional Matter Science, National Chiao Tung University, Hsinchu 30010, Taiwan

E-mail: shih-wen.huang@maxiv.lu.se, ychuang@lbl.gov and ago@cc.nctu.edu.tw

Received 13 November 2018, revised 13 January 2019
Accepted for publication 8 February 2019
Published 8 March 2019

Abstract

X-ray absorption spectroscopy (XAS) is performed to study changes in the electronic structures of colossal magnetoresistance (CMR) and charged ordered (CO) $La_{1-x}Ca_xMnO_3$ manganites with respect to temperature. The pre-edge features in O and Mn *K*-edge XAS spectra, which are highly sensitive to the local distortion of MnO_6 octahedral, exhibit contrasting temperature dependence between CMR and CO samples. The seemingly counter-intuitive XAS temperature dependence can be reconciled in the context of polarons. These results help identify the most relevant orbital states associated with polarons and highlight the crucial role played by polarons in understanding the electronic structures of manganites.

Keywords: colossal magnetoresistance, x-ray absorption, polaron

1. Introduction

Manganese oxides $R_{1-x}A_xMnO_3$ (R = La, Pr, ... etc; A = Ca, Sr, Ba) have been extensively studied over past decades to understand their rich phase diagrams manifested by interactions between lattice, charge, spin, and orbital degrees of freedom. These interactions lead to several intriguing phenomena such as colossal magnetoresistance (CMR), electronic phase separation, electronic ordering. These compounds not only offer the opportunities for researchers to examine the nature of electronic correlations, but also have potential applications in next generation electronic devices. Despite extensive studies on these manganites, the detailed picture about the mechanisms behind manifestation of these phase diagrams is still not fully clear [1–4].

$La_{1-x}Ca_xMnO_3$ is a prototypical manganite showing a complex phase diagram, which is reproduced in figure 1(a) [1]. The undoped parent compound $LaMnO_3$ ($x = 0$) is an A-type antiferromagnetic insulator that exhibits alternating $d_{3x^2-r^2}/d_{3y^2-r^2}$ orbital ordering below $T_{OO} \sim 780$ K. At low doping regime ($x \leqslant 0.2$), the material remains insulating but the low temperature magnetic ground state changes from antiferromagnetic to ferromagnetic. With Ca doping in between ~0.2 and ~0.5, upon cooling, the material undergoes a paramagnetic (PM) to ferromagnetic (FM) transition accompanied by an insulator to metal transition. This insulator-metal

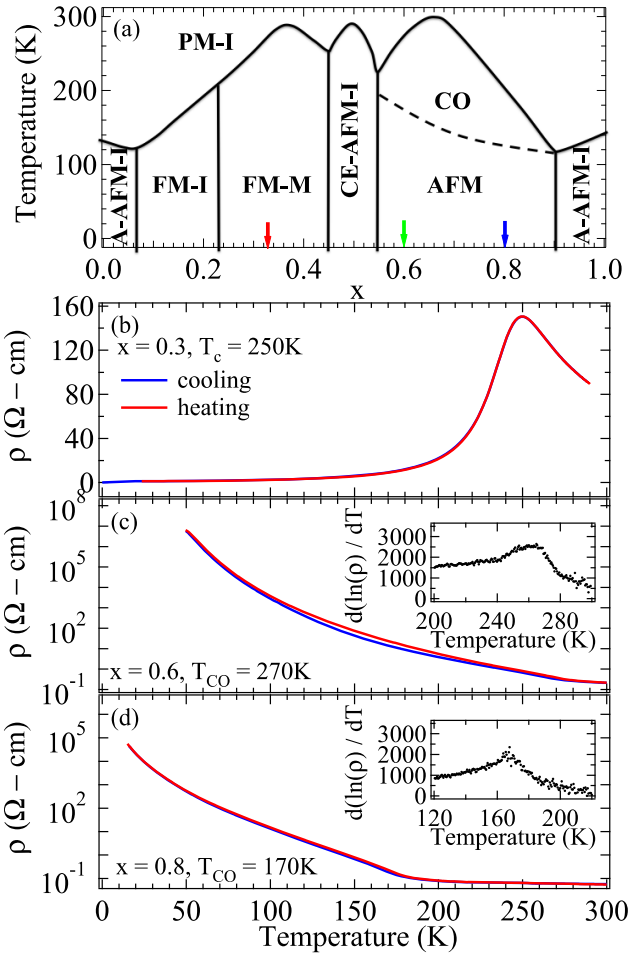

Figure 1. (a) Schematic phase diagram of $La_{1-x}Ca_xMnO_3$. Color arrows indicate the doping levels studied in this work. (b)–(d) Temperature dependence of resistivity curves of $La_{1-x}Ca_xMnO_3$ ($x = 0.3, 0.6$, and 0.8). The insets show the derivative $d[ln(\rho(T))]/dT$ of the cooling curve.

transition, when tuned by external magnetic field, can lead to the so-called CMR effect. When Ca doping is higher than 50% ($x \geqslant 0.5$), the high temperature phase boundary mimics that at low doping regime; however, the ground state is now a charge ordered (CO) antiferromagnetic insulator.

The CMR effect has disparate magnitude for different manganite families and can be induced by numerous perturbations besides magnetic field [5, 6]. The versatility in inducing CMR effect implies the coexistence of competing ground states with proximate energies. Similar nature is also found in CO state where ordering periodicity can vary with hole doping. In that regard, the Zener double-exchange interaction from the perspective of carrier hopping only provides a qualitative description for CMR effect. Other mechanisms, such as polaronic effect arising from strong electron-phonon coupling, the Jahn–Teller distortion (JTD) of MnO_6 octahedra, and electronic phase separation, have been suggested to be indispensable for manganite physics [2–4, 7].

In $LaMnO_3$, Mn^{3+} has four $3d$ electrons arranged in high spin configuration $t^3_{2g\uparrow}e^1_{g\uparrow}$ due to strong Hund's first rule to maximize the total spin quantum number. The singly occupied $e^1_{g\uparrow}$ state favors the Jahn–Teller (JT) effect to lower the energy. However, when holes are doped into $e^1_{g\uparrow}$ state, the JT effect can be suppressed or even quenched to give way to metallicity. JTD can also display long range coordinated nature, which results in a long-range ordering of occupied $e^1_{g\uparrow}$ below the CO transition temperature at high doping level when the material only needs to incorporate fewer distorted Mn^{3+} sites. As such, various types of Jahn–Teller polarons, e.g. correlated versus uncorrelated, small versus large, dynamic versus static, can play important roles in phase transitions seen in the phase diagram [4, 8–11].

The present work possesses a twofold novelty: (1) the understanding of the relation between JTD and the relevant orbital states, which was not specified in the literature; (2) a systematic way to achieve this understanding via the *temperature dependent* x-ray absorption spectroscopy (XRS). We elaborate both points in the following paragraph.

(1) Albeit with previous studies of Jahn–Teller polarons and their influence on transport properties [12–22], the evolution of electronic structures with respect to JT distortion remains elusive. This knowledge appears even more precious with the recent development of multiferroic manganites, where the electronic structure due to JTD plays a crucial role for the magnetoelectric effect. A better understanding of this issue through the present work should also advance further applications of multiferroics and manganites [23]. (2) Previous temperature dependent O *K*-edge XAS studies were scattered and only focused on CMR samples [24–27]. The present work covers both CMR and CO compounds. Moreover, we have measured both O *K*-edge and Mn *K*-edge XAS on the same samples to obtain a more comprehensive picture. This complete comparison was absent in the previous studies [28–30]. We will also emphasize the opposite and seemingly counter-intuitive temperature dependences in O and Mn *K*-edge XAS spectra between CMR and CO $La_{1-x}Ca_xMnO_3$ samples. This intriguing contrast was not reported previously, and can be reconciled in the context of polarons. The present results highlight their crucial roles in manganites.

2. Experiment

Single phase polycyrstalline $La_{1-x}Ca_xMnO_3$ samples were prepared by solid state reaction method. High purity (purity $\geqslant$ 99.99%) stoichiometric La_2O_3, $MnCO_3$, and $CaCO_3$ were first mixed in an agate mortar and then heated in air at 1200 °C for 8 h. In the thermal processes, the temperature ramping rate was ≈2.5 °C min^{-1}. After annealing, the specimens were reground and the same procedure was repeated for three times. For each time, the maximum temperature was increased by 10 °C. After three thermal cycles, the powder was pressed into pellet form followed by another annealing in air at 1200 °C for 12 h. The samples were checked by room temperature x-ray powder diffraction (data not shown) to ensure the absence of any secondary phase.

XAS measurements were carried out at National Synchrotron Radiation Reach Center (NSRRC) in Taiwan. O *K*-edge measurements were performed at HSGM (20 A) beamline with 0.1 eV energy resolution. Mn *K*-edge spectra

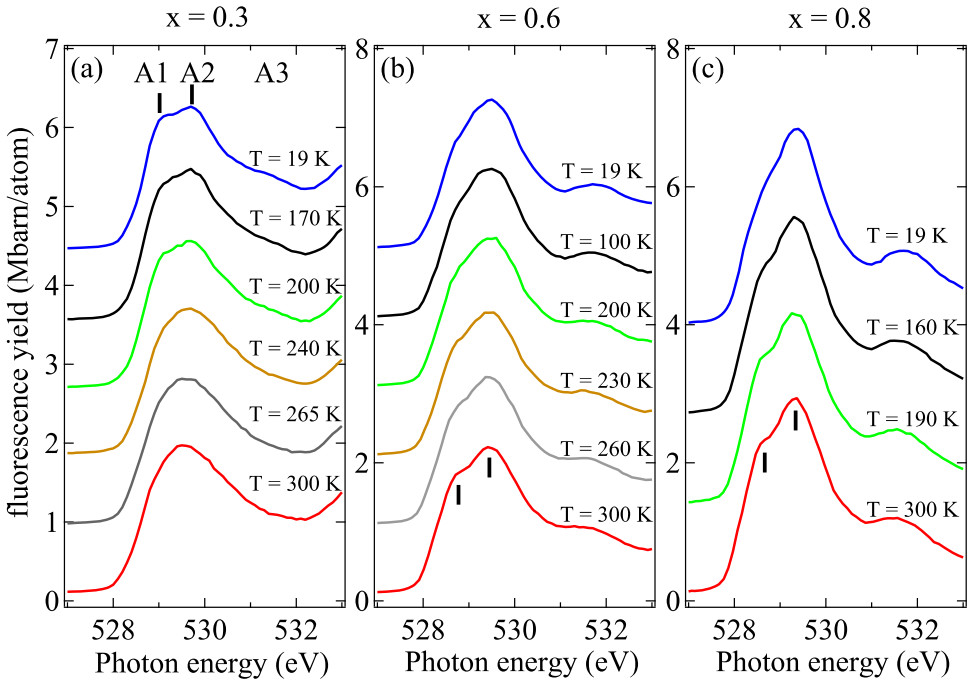

Figure 2. Temperature dependence of the pre-edge region of O *K*-edge XAS spectra measured on (a) CMR $La_{0.7}Ca_{0.3}MnO_3$ ($x = 0.3$) and CO samples, (b) $La_{0.4}Ca_{0.6}MnO_3$ ($x = 0.6$), and (c) $La_{0.2}Ca_{0.8}MnO_3$ ($x = 0.8$). The T_C and T_{CO} for $x = 0.3$, 0.6, and 0.8 samples are 250 K, 270 K, and 170 K, respectively.

were recorded at beamline 17C. Using Si (1 1 1) double crystal monochromator, the energy resolution was better than 1.4 eV. O and Mn *K*-edge spectra were recorded by measuring the bulk sensitive florescence-yield and transmission using micro-channel plate (MCP) detector and Lytle detector, respectively. The resistivity measurements were carried out using four point method in cooling and warming processes.

3. Results

Figure 1 shows the resistivity curves of $La_{0.7}Ca_{0.3}MnO_3$ (CMR, $x = 0.3$), $La_{0.4}Ca_{0.6}MnO_3$ (CO, $x = 0.6$), and $La_{0.2}Ca_{0.8}MnO_3$ (CO, $x = 0.8$) samples. Our results are consistent with those in the literatures [31–33]. Upon cooling, the $x = 0.3$ sample shows a paramagnetic insulator (PMI) to ferromagnetic metal (FMM) transition at $T_C \sim 250$ K determined by the maximum of resistivity curve $\rho(T)$ (figure 1(b)). For $x = 0.6$ (figure 1(c)) and 0.8 (figure 1(d)) samples, an abrupt increase in resistivity at $T_{CO} = 270$ K and $T_{CO} = 170$ K is attributed to the emergence of charge ordering (see insets for the derivative $d[\ln(\rho(T))]/dT$ of cooling curves). Presence of CO also leads to hysteresis in $\rho(T)$.

The temperature dependent O *K*-edge XAS spectra from these samples are shown in figure 2. All spectra were normalized using the spectral weight integrated between 600 eV and 620 eV, far above absorption edge, and the self-absorption effect was corrected. The strong hybridization between O 2*p* and Mn 3*d* orbitals (σ and π bonding for metal and ligand orbitals with E_g and T_{2g} symmetry, respectively; with D_{4h} site symmetry, the Mn orbitals involved will have b_{2g} (d_{xy}), e_g (d_{xz} and d_{yz}), a_{1g} ($d_{3z^2-r^2}$), and b_{1g} ($d_{x^2-y^2}$) symmetry) leads to the pre-edge structure below ~533 eV [34]. There are three features that can be identified around 529.2 eV (A_1), 529.7 eV (A_2), and 531.5 eV (A_3) in the $T = 19$ K spectrum of $x = 0.3$ sample (these energies depend on doping level x.) These features are associated with dipole transitions to the majority e_g ($e_{g\uparrow}$), minority t_{2g} ($t_{2g\downarrow}$), and minority e_g ($e_{g\downarrow}$) states, respectively (see the schematic energy diagram in figure 3) [35]. By comparing these spectra, one finds that the intensity of A_3 is enhanced dramatically in Mn^{4+} rich compound ($x = 0.8$) and the total integrated intensity in (527.5 eV, 532 eV) energy window is also larger. This observation indicates the stronger covalent bonding between Mn and O orbitals at higher doping level x. In the following, we focus on features A_1 and A_2 which are the keys to the present scenario.

4. Analyses of the temperature dependent O *K*-edge XAS

To gain insight on the quantitative behaviors of temperature dependent O *K*-edge XAS spectra, we use three Lorentzian functions on top of a monotonic background to fit XAS spectra between 527.5 eV and 532 eV. To constrain the fitting, the ratio between peak area of A_1 and A_2 is held constant, which inherently assumes that other subtle effects such as variations in Mn–O orbital hybridization with respect to temperature are neglected. We emphasize that the fitting is mainly used to draw out the generic trend in temperature and doping dependence of electronic structures. Without accurate estimate on crystal field parameters like $10Dq$, Ds, and Dt with respect to doping, and the broadening of spectral width by core hole lifetime, detailed quantitative analysis will be restrictive. The fitting results are summarized in figure 4. Here, we use ΔE_x and $W_{x(A_i)}$ to denote the energy separation between A_1 ($e_{g\uparrow}$) and A_2 ($t_{2g\downarrow}$) and the width of features $A_{i=1,2}$ for sample with doping x, respectively.

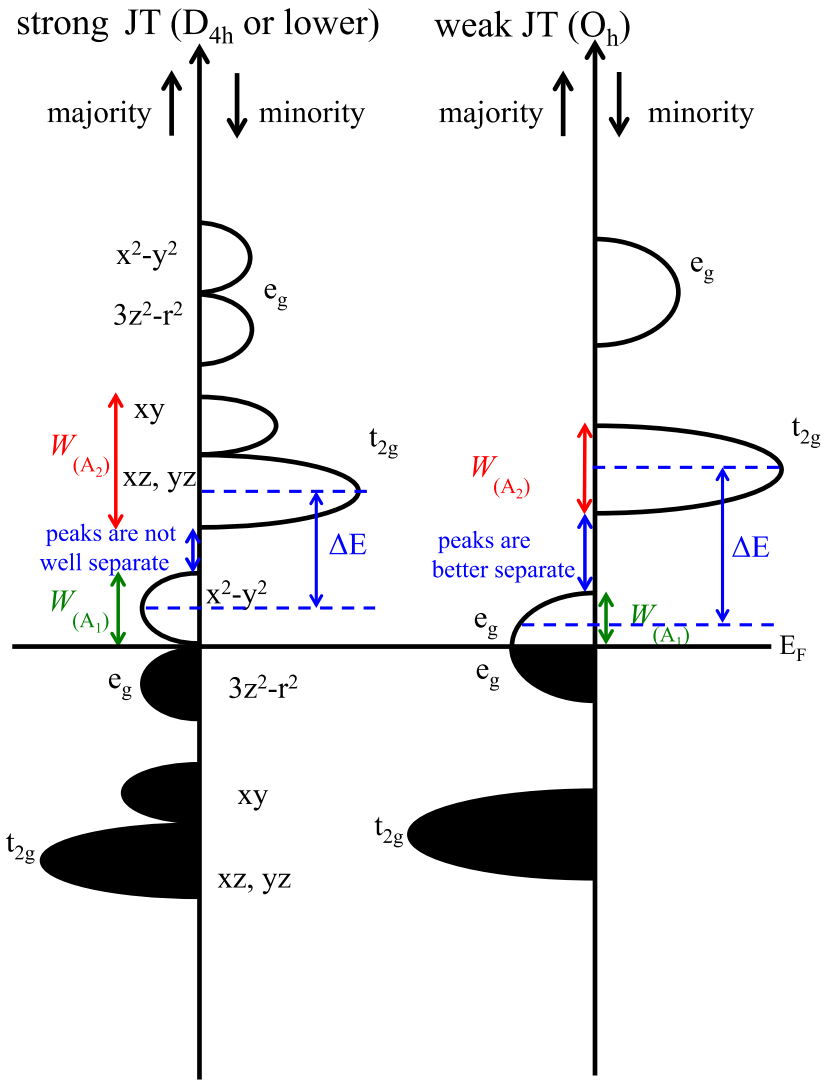

Figure 3. Schematic energy diagram of the Mn 3*d* states with strong (left) and weak (right) Jahn–Teller distortion. The change in energy scale is exaggerated to qualitatively demonstrate the scenario.

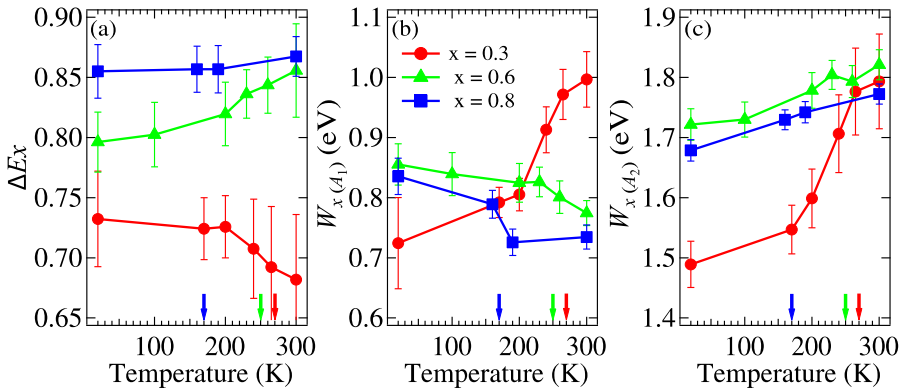

Figure 4. Lorentzian function fitting results showing (a) the energy separation between features A_1 and A_2, and the peak width of (b) A_1 and (c) A_2 for $x = 0.3$ (red circles), 0.6 (green triangles), and 0.8 (blue squares) samples. The transition temperatures T_C and T_{CO} are indicated by colored arrows.

4.1. Temperature dependence of ΔE_x

The energy separation between A_1 and A_2 displays distinct temperature and doping dependence. For $x = 0.3$ sample (figure 2(a)), the separation is better resolved at low temperatures whereas for $x = 0.6$ (figure 2(b)) and 0.8 (figure 2(c)) samples, it is better resolved at high temperatures. From figure 4(a), one can see that when the temperature is lowered, the energy separation in $x = 0.3$ sample ($\Delta E_{0.3}$, red circles) increases monotonically. On the other hand, the trend is opposite for

$x = 0.6$ sample ($\Delta E_{0.6}$, green triangles). As for $x = 0.8$ sample ($\Delta E_{0.8}$, blue squares), it remains nearly temperature independent because the fraction of Mn^{3+} is greatly reduced. This finding seems to be unusual since the high-temperature state for all samples is a PM. This point will be discussed later on. Furthermore, the cause for the splitted pre-edge features in CMR samples was previously debated: Dessau *et al* [27] suggested that these two features at low temperature originate from the broken degeneracy of e_g states by the distortion of MnO_6 octahedra, while Toulemonde *et al* [36] concluded from their studies on $Pr_{0.7}Sr_{0.3}MnO_3$ and $Pr_{0.7}Ca_{0.15}Sr_{0.15}MnO_3$ that it is the consequence of insulator-metal transition likely associated with weakening of Jahn-Teller distortion.

With the energetics of Mn 3*d* orbitals depicted in figure 3, we propose a unified scenario to understand the distinct temperature dependence of ΔE_x for both CMR and CO samples, and later for that of $W_{x(A_i)}$. In perovskite manganites, the MnO_6 octahedron has O_h site symmetry where crystal field lifts the degenerate 3*d* orbitals into triply degenerate t_{2g} (d_{xy},d_{yz} and d_{xz}) states lying lower in energy and double degenerate e_g ($d_{x^2-y^2}$ and $d_{3z^2-r^2}$) states lying at higher energy. The energy separation of two sub-manifolds is $10Dq$. The exchange interaction (J_{ex}) further splits them into spin up (↑) and spin down (↓) states. With presence of JTD around Mn^{3+} sites, the symmetry is further lowered to D_{4h} and degenerate e_g (t_{2g}) orbitals are further splitted into $d_{3z^2-r^2}$ and $d_{x^2-y^2}$ ($d_{xz/yz}$ and d_{xy}) orbitals denoted as a_{1g} and b_{1g} (e_g and b_{2g}). The filling of Mn 3*d* orbitals with strong Hund's first rule coupling can be schematically illustrated in figure 3 with strong (left panel) or weak (right panel) JTD.

How does the strength of JTD lead to the temperature dependence of ΔE_x that we observed in figure 4(a)? With Ca doping, the magnitude of JTD along with competition between J_{ex} and $10Dq$ will considerably modify the energy splitting between $e_{g\uparrow}$ and $t_{2g\downarrow}$ states [35, 36]. For $x = 0.3$ sample, local JTD is weakened in FMM state (right panel of figure 3) compared to that in PMI state (left panel of figure 3). This weaker JTD leads to a smaller energy splitting between $d_{3z^2-r^2}$ and $d_{x^2-y^2}$ orbitals (as well as in between $d_{xz/yz}$ and d_{xy}) [13, 17, 24, 37, 38]. As a consequence, the edges of $e_{g\uparrow}$ and $t_{2g\downarrow}$ bands are more distant to each another, so is the peak of density of states (DOS). These effects are highlighted in figure 3. Thus if there are no drastic changes in $10Dq$ and J_{ex}, for $x = 0.3$ sample, ΔE_x is expected to be smaller at high temperatures than at low temperatures where JTD is weaker, consistent with what is seen in figure 4(a).

For $x = 0.6$ and 0.8, no detailed study of temperature dependent O *K*-edge XAS was reported until now. Intriguingly, the results in figure 4(a) also fit into the universal picture of figure 3. For $x = 0.6$ sample above T_{CO}, ferromagnetic spin fluctuations dominate. With decreasing temperature, these fluctuations are replaced by antiferromagnetic interaction that localizes the carriers. The antiferromagnetic insulating CO state at low temperatures is with an enhanced local JTD, which pushes the edges of $e_{g\uparrow}$ and $t_{2g\downarrow}$ states closer to each other and leads to a smaller ΔE_x as depicted in the left panel of figure 3 [38–41]. On the other hand, the weaker JTD at high temperature associated with the presence of short-range ferromagnetic clusters will be analogous to that of CMR sample at low temperature, hence the splitting between $e_{g\uparrow}$ and $t_{2g\downarrow}$ or ΔE_x becomes larger (right panel of figure 3). As for $x = 0.8$ sample, the fraction of Mn^{3+} is significantly reduced compared with that of Mn^{4+}. The enhanced JTD in CO state is thus not expected to significantly shift the centroid (or DOS peak) of $e_{g\uparrow}$ states relative to that of $t_{2g\downarrow}$ state. This explains why the temperature dependence of ΔE_x is weaker for $x = 0.8$ sample than that of $x = 0.6$.

4.2. Temperature dependence of $W_{x(A_i)}$

Noticeable temperature dependences in $W_{x(A_i)}$ can be seen in figures 4(b) and (c). For $x = 0.3$ sample, both $W_{0.3(A_1)}$ and $W_{0.3(A_2)}$ show the monotonic decrease from 300 K to 19 K. This temperature dependence can be naturally explained by the proposed universal scenario. Local JTD is weakened in FMM state (right panel of figure 3) compared to that in PMI state (left panel of figure 3) [38, 42]. This weak JTD can reduce the splitting of $e_{g\uparrow}$ and $t_{2g\downarrow}$ states, leading to a smaller width for both A_1 and A_2 (see red and green arrows, respectively.) In addition, in FMM state, the higher electron itinerancy can help reduce the spatial inhomogeneity in electronic structures. To first order, the binding energies of Mn 3*d* orbitals relative to the core levels will depend strongly on the valence state of Mn and its environment. Thus if the electronic structures of Mn sites probed by XAS are spatially inhomogeneous, the XAS spectral features are expected to become broader. The reduced $W_{0.3(A_1)}$ and $W_{0.3(A_2)}$ suggest that FMM state is likely more homogeneous compared with PMI state. Such spatial homogeneity in local structure is also supported by the smaller Debye–Waller width parameter σ^2_{Mn-O} in FMM state [38, 40].

On the other hand, charge ordering develops below T_{CO} in $x = 0.6$ and 0.8 samples, and JTD becomes strong. Consequently, $W_{0.6(A_1)}$ and $W_{0.8(A_1)}$ increase with decreasing temperature. It is noted that both $W_{0.6(A_2)}$ and $W_{0.8(A_2)}$ simply decrease with decreasing temperature, and their values are comparable to that of $W_{0.3(A_2)}$ at room temperature. Likely the correlated polarons have stronger effects on e_g state than on t_{2g} states for $x = 0.6$ and 0.8 samples. This suggestion may require detailed theoretical calculations for further understanding.

5. The temperature dependent Mn *K*-edge XAS

The pre-edge features in Mn *K*-edge XAS spectra originate from the quadrupole transitions from Mn 1*s* to 3*d* orbitals and are thus sensitive to local structural distortion [28, 29, 43, 44]. In figure 5(a), the Mn *K*-edge XAS spectra from these samples at 300 K and the overall spectral lineshape are in good agreement with the literature [28–30]. With increasing Ca doping, the main peak around 6556 eV shifts towards higher energy due to higher average Mn valency. The contrasting temperature dependence, analogous to that in O *K*-edge XAS spectra, can also be seen in Mn *K*-edge XAS spectra. The pre-edge features become stronger with increasing Ca doping, indicative of stronger covalent bonding between the Mn and O orbitals.

In figures 5(e)–(g), we compare the pre-edge features at 300 K (red curves) and 18 K (blue curves), and their differences are plotted in the bottom panels. Two main features B_1 and B_2 can be identified in the difference spectra in this region. With decreasing temperature, B_1 and B_2 exhibit opposite dependence: one increases at the expense of the other. Furthermore, we see that the behavior of $x = 0.3$ (figure 5(e)) sample is also opposite compared with that of $x = 0.6$ (figure 5(f)) and 0.8 (figure 5(g)) samples. Qian *et al* [29] attributed the changes of pre-edge feature upon cooling to the change of averaged Mn valence.

6. Discussion

Although the high temperature state in the phase diagram in figure 1 is called PMI in general, there is still a subtle difference in term of Jahn–Teller polaronic effect between different doping levels. According to the values of ΔE_x in figure 4(a) at 300 K, JTD is significantly weakened when $x > 0.5$. This suggestion is consistent with the reports by local probes such as extended x-ray absorption fine structure that the monotonic increase in the Mn–O peak intensity in coordination shell with x was interpreted as the relaxation of JTD at high Ca doping [38, 40, 45]. The agreement between findings from structural probes and XAS highlights the influence of Jahn–Teller polaronic effect on the electronic structure of mixed-valent manganites, and the prediction power of our universal picture of figure 3.

At room temperature, both $W_{0.6(A_1)}$ and $W_{0.8(A_1)}$ are smaller than $W_{0.3(A_1)}$, which is again consistent with the relaxation of JTD at high Ca doping, and in accord with the behaviors of ΔE_x seen in figure 4(a) as discussed above. At low temperatures, both $W_{0.6(A_1)}$ and $W_{0.8(A_1)}$ are larger than $W_{0.3(A_1)}$, which is also in agreement with the proposed universal scenario. Interestingly, the change in the values of $W_{x(A_i)}$ is larger than that in the energy separation ΔE_x (particularly for $x = 0.3$ sample), an effect that was overlooked in previous studies. We speculate that such width behavior may be a more important factor in understanding the O *K*-edge spectra and other physical properties especially at low doping x regime where large or intermediate bandwidth manganites that exhibit FMM states. For example, this effect implies that the carriers in FMM state of $La_{1-x}Ca_xMnO_3$ are easier to be localized due to defects or impurities than in ordinary metals.

Finally, we focus on the pre-edge features in Mn *K*-edge XAS spectra. In the present study, the pre-edge features in both O and Mn *K*-edge XAS spectra show the contrasting temperature dependence between CMR ($x = 0.3$) and CO ($x = 0.6$ and 0.8) samples. Furthermore, the change of Mn valence state was not observed in figures 5(b)–(d) *and* the O *K*-edge XAS spectra. Hence we believe that other mechanism is responsible for the temperature dependence of B_1. Based on Elfimov *et al* [46] and Hozoi *et al* [47], B_1 can be assigned to the quadrupole transition to $e_{g\uparrow}$ state through orbital hybridization with the neighboring Mn sites. Such hybridization will involve bridging O atoms and the mobility of e_g electrons, and

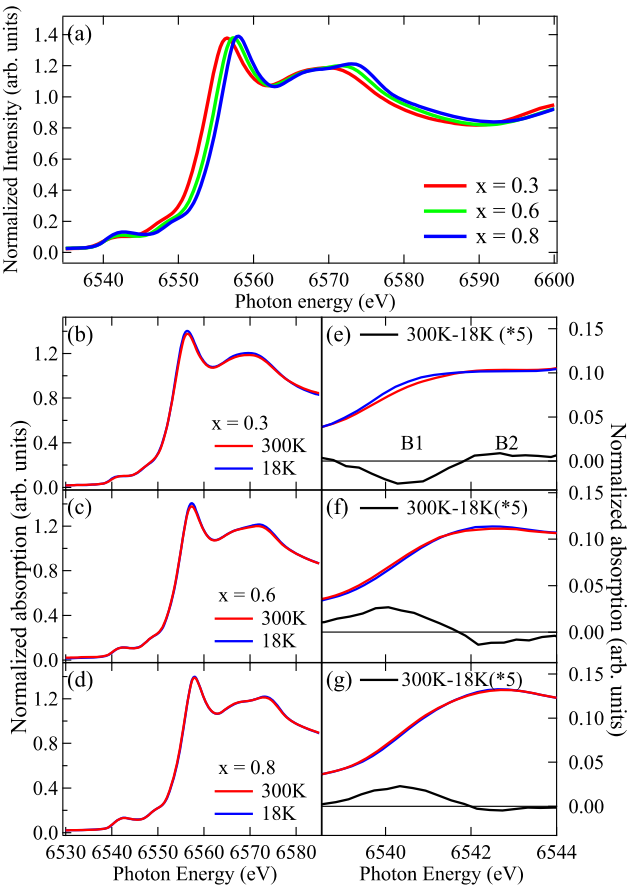

Figure 5. (a) Normalized Mn *K*-edge XANES spectra of $La_{1-x}Ca_xMnO_3$ ($x = 0.3$, 0.6, and 0.8) measured at 300 K. (b)–(d) The *K*-edge XAS spectra of $La_{1-x}Ca_xMnO_3$ with $x = 0.3$, 0.6, and 0.8 recorded at 300 K (red) and 18 K (blue). (e)–(g) The expanded pre-edge region which covers from 6538 eV to 6544 eV. The difference spectra (black) are shown in bottom panels.

can be a key factor in determining the intensity of this feature. By comparing the O *K*-edge XAS data in figure 2 and considering the electronic localization with JTD and tilting of MnO_6 octahedral (buckling of Mn–O–Mn bond) in the CO state, it is expected that the intensity of B_1 will be enhanced (suppressed) in the FMM (CO) compared to the PMI state at 300 K. The simulated spectra with strong and weak Jahn–Teller distortion are shown in the supplementary material (available online at stacks.iop.org/JPhysCM/31/195601/mmedia).

7. Conclusion

In summary, the temperature and doping dependence of O and Mn *K*-edge XAS spectra show that the electronic structures of mixed valent manganites are highly sensitive to the local distortion of MnO_6 octahedra (Q_2 and Q_3 JTD and Q_1 breathing mode). The contrasting temperature dependence of XAS spectra seen in the colossal magnetoresistance and charge-ordered $La_{1-x}Ca_xMnO_3$ manganites can be reconciled by a scenario based on the energetics of Mn 3*d* orbitals. With this scenario, we highlight the important role of JT polarons in understanding the electronic structures of manganites, and specify the orbital states most relevant to the correlated

polarons. Although the ferromagnetic metallic state is realized below the CMR transition, the Jahn–Teller polaronic effect remains noticeable. The success in the present work suggests that similar studies can be extended to other doping levels x, and/or manganite families beyond $La_{1-x}Ca_xMnO_3$ to elucidate the effects of Jahn–Teller polaron on the electronic structure. In addition, this x-ray methodology in identifying the signature of polarons may be useful for studying material classes such as thin films, nanoparticles, … etc where x-ray cross-section has the advantage.

Acknowledgment

The Advanced Light Source is supported by the Director, Office of Science, Office of Basic Energy Sciences, of the US Department of Energy under Contract No. DE-AC02-05CH11231. Work by YTL and JYL was financially supported by the MOST of Taiwan, under the Grant 103-2112-M-009-007-MY3 and the Center for Emergent Functional Matter Science of National Chiao Tung University from The Featured Areas Research Center Program within the framework of the Higher Education Sprout Project by the Ministry of Education (MOE) in Taiwan.

ORCID iDs

S W Huang https://orcid.org/0000-0003-0349-4125
J-Y Lin https://orcid.org/0000-0002-3638-0020

References

[1] Cheong S W and Hwang H Y 2000 Ferromagnetism versus charge/orbital ordering in mixed-valent manganites *Colossal Magnetoresistive Oxides* ed Y Tokura (London: Gordon and Breach)
[2] Tokura Y 2006 *Rep. Prog. Phys.* **69** 797
[3] Dagotto E, Hotta T and Moreo A 2001 *Phys. Rep.* **344** 1
[4] Dagotto E 2005 *New J. Phys.* **7** 67
[5] Li T, Patz A, Mouchliadis L, Yan J, Lograsso T A, Perakis I E and Wang J 2013 *Nature* **496** 69–73
[6] Beaud P *et al* 2014 *Nat. Mater.* **13** 923–7
[7] Millis A J, Littlewood P B and Shraiman B I 1995 *Phys. Rev. Lett.* **74** 5144
[8] Dai P, Fernandez-Baca J A, Wakabayashi N, Plummer E W, Tomioka Y and Tokura Y 2000 *Phys. Rev. Lett.* **85** 2553
[9] Adams C P, Lynn J W, Mukovskii Y M, Arsenov A A and Shulyatev D A 2000 *Phys. Rev. Lett.* **85** 3954
[10] Lynn J W, Erwin R W, Borchers J A, Huang Q, Santoro A, Peng J-L and Li Z Y 1996 *Phys. Rev. Lett.* **76** 4046
[11] Şen C, Alvarez G and Dagotto E 2007 *Phys. Rev. Lett.* **98** 127202
[12] Zhao G-M, Conder K, Keller H and Müller K A 1996 *Nature* **381** 676
[13] Billinge S J L, DiFrancesco R G, Kwei G H, Neumeier J J and Thompson J D 1996 *Phys. Rev. Lett.* **77** 715
[14] Louca D, Egami T, Brosha E L, Röder H and Bishop A R 1997 *Phys. Rev.* B **56** R8475
[15] Shimomura S, Wakabayashi N, Kuwahara H and Tokura Y 1999 *Phys. Rev. Lett.* **83** 4389
[16] Vasiliu-Doloc L, Rosenkranz S, Osborn R, Sinha S K, Lynn J W, Mesot J, Seeck O H, Preosti G, Fedro A J and Mitchell J F 1999 *Phys. Rev. Lett.* **83** 4393
[17] Nelson C S *et al* 2001 *Phys. Rev.* B **64** 174405
[18] Kim K H, Gu J Y, Choi H S, Park G W and Noh T W 1996 *Phys. Rev. Lett.* **77** 1877
[19] Kim K H, Jung J H and Noh T W 1998 *Phys. Rev. Lett.* **81** 1517
[20] Okimoto Y, Katsufuji T, Ishikawa T, Urushibara A, Arima T and Tokura Y 1995 *Phys. Rev. Lett.* **75** 109
[21] Quijada M, Černe J, Simpson J R, Drew H D, Ahn K H, Millis A J, Shreekala R, Ramesh R, Rajeswari M and Venkatesan T 1998 *Phys. Rev.* B **58** 16093
[22] Moshnyaga V *et al* 2014 *Phys. Rev.* B **89** 024420
[23] Haw S-C, Lee J-M, Chen S-A, Lu K-T, Lee M-T, Pi T-W, Lee C-H, Hu Z and Chen J-M 2016 *Dalton Trans.* **45** 16393
[24] Mannella N, Rosenhahn A, Watanabe M, Sell B, Nambu A, Ritchey S, Arenholz E, Young A, Tomioka Y and Fadley C S 2005 *Phys. Rev.* B **71** 125117
[25] Pellegrin E, Tjeng L H, de Groot F M F, Hesper R, Sawatzky G A, Moritomo Y and Tokura Y 1997 *J. Electron. Spectrosc. Relat. Phenom.* **86** 115
[26] Park J-H, Kimura T and Tokura Y 1998 *Phys. Rev.* B **58** R13330
[27] Dessau D S, Chuang Y D, Gromko A, Saitoh T, Kimura T and Tokura Y 2001 *J. Electron. Spectrosc. Relat. Phenom.* **117–8** 265
[28] Bridges F, Booth C H, Kwei G H, Neumeier J J and Sawatzky G A 2000 *Phys. Rev.* B **61** R9237
[29] Qian Q, Tyson T A, Kao C-C, Croft M, Cheong S-W and Greenblatt M 2000 *Phys. Rev.* B **62** 13472
Qian Q, Tyson T A, Kao C-C, Croft M, Cheong S-W and Greenblatt M 2003 *Phys. Rev.* B **68** 014429
[30] Bridges F, Booth C H, Anderson M, Kwei G H, Neumeier J J, Snyder J, Mitchell J, Gardner J S and Brosha E 2001 *Phys. Rev.* B **63** 214405
[31] Markovich V, Fita I, Puzniak R, Rozenberg E, Martin C, Wisniewski A, Yuzhelevski Y and Gorodetsky G 2005 *Phys. Rev.* B **71** 134427
[32] Gordon I, Wagner P, Das A, Vanacken J, Moshchalkov V V, Bruynseraede Y, Schuddinck W, Van Tendeloo G, Ziese M and Borghs G 2000 *Phys. Rev.* B **62** 11633
[33] Abbate M *et al* 1992 *Phys. Rev.* B **46** 4511
[34] Kettle S F A 1996 *Physical Inorganic Chemistry: a Coordination Chemistry Approach* (Berlin: Springer)
[35] Tsai Y T, Chang W J, Huang S W, Lin J-Y, Lee J Y, Chen J M, Wu K H, Uen T M, Gou Y S and Juang J Y 2009 *Physica* B **404** 1404
[36] Toulemonde O, Millange F, Studer F, Raveau B, Park J-H and Chen C-T 1999 *J. Phys.: Condens. Matter* **11** 109
[37] Lanzara A, Saini N L, Brunelli M, Natali F, Bianconi A, Radaelli P G and Cheong S-W 1998 *Phys. Rev. Lett.* **81** 878
[38] Booth C H, Bridges F, Kwei G H, Lawrence J M, Cornelius A L and Neumeier J J 1998 *Phys. Rev.* B **57** 10440
[39] Subías G, García J, Blasco J and Proietti M G 1998 *Phys. Rev.* B **57** 748
[40] Subías G, García J, Blasco J, Sánchez M C and Proietti M G 2002 *J. Phys.: Condens. Matter* **14** 5017
[41] Radaelli P G, Cox D E, Marezio M and Cheong S-W 1997 *Phys. Rev.* B **55** 3015
[42] Božin E S, Schmidt M, DeConinck A J, Paglia G, Mitchell J F, Chatterji T, Radaelli P G, Proffen Th and Billinge S J L 2007 *Phys. Rev. Lett.* **98** 137203
[43] Subías G, García J, Proietti M G and Blasco J 1997 *Phys. Rev.* B **56** 8183

[44] Takahashi M, Igarashi J and Flude P 2000 *J. Phys. Soc. Japan* **69** 1614
[45] Bindu R, Pandey S K, Kumar A, Khalid S and Pimpale A V 2005 *J. Phys.: Condens. Matter* **17** 6393
[46] Elfimov I S, Anisimov V I and Sawatzky G A 1999 *Phys. Rev. Lett.* **82** 4264
[47] Hozoi L, de Vries A H and Broer R 2001 *Phys. Rev.* B **64** 165104